Typesetting a Book in MS Word Using the WSPC Book Style *1*

Chapter 1

SERS Theory: The Chemical Effect of Rhodamine 6G Adsorption on Silver Surfaces on its Raman Spectrum

Lindsey R. Madison, Mark A. Ratner, and George C. Schatz

Department of Chemistry, Northwestern University, Evanston, IL, 60208-3113

g-schatz@northwestern.edu

1.1 Introduction

The SERS spectra of small organic molecules can be very sensitive to the physisorption or chemisorption of the molecules onto metallic surfaces. However it is challenging to model the results, as typical SERS substrates have a broad distribution of possible surface sites, and the populations of these sites and the SERS enhancement factors associated with them are very difficult to determine, especially when electromagnetic hot spots dominate the observed spectra. However it is important to account for these effects if one is to make a quantitative interpretation of measured SERS spectra. Indeed, the influence of different sites is important to both the electromagnetic and chemical mechanisms in SERS, where the former mechanism is concerned with local field enhancement effects arising from plasmon excitation, while the latter arises from the effect of chemisorption induced charged transfer on the Raman

intensities, as can be modeled using static limit Raman intensity calculations[1]. Extensive studies have been performed on simple organics like pyridine bound to gold and silver clusters, and it was found that both the chemical and electrodynamic enhancement factors associated with binding pyridine in various orientations result in noticeable changes in the SERS spectra compared to the gas phase spectrum of pyridine.[2]

One of the most important benchmark molecules for SERS and TERS studies is Rhodamine 6G (R6G). This is a strongly fluorescent dye molecule in solution, but when adsorbed onto SERS substrates, its fluorescence is quenched, and the resulting SERS intensities are among the largest observed for any molecule. As a result R6G has played a crucial role in the development of single molecule SERS, and in the development of SERS substrates. [3, 4]

Previously, the SERS spectrum of R6G has been modeled as if it were a gas phase molecule. Jensen and Schatz[5] incorporated resonant effects as well as vibronic effects and found that resonance excitation to the S_1 excited state of R6G resulted in good agreement with spectra obtained from SERS experiments. In another study, intermolecular charge transfer was studied with R6G bound to a Ag_2 cluster.[6] It is unclear if a cluster model as small as two silver atoms can accurately capture the surface effects of a nanoparticle with thousands of atoms.

Recent single molecule, ultra high vacuum, tip enhanced Raman spectroscopy (SM-UHV-TERS) measurements for R6G[3] were moderately reproduced by gas phase resonance Raman calculations. Of particular importance in this work was the comparison of TERS spectra at room temperature with those at a low temperature of 10K. It was found that lowering the temperature led to both sharpening of the vibrational spectra, and shifts in the spectra (up to 20 cm^{-1} with some lines shifting red, some blue and some not at all), suggesting that the molecule transitions from a largely gas phase molecule at room temperature to being strongly chemisorbed at 10K. A potential energy distribution analysis performed by Chulhai and Jensen[3] showed that the modes that were shifted from the gas phase had vibrational activity associated with the ethylamine component of R6G, which is the likely moiety associated with binding of R6G

to the metal surface. However the metal surface was not incorporated into the Raman calculations.

What remains unresolved concerning the SM-UHV-TERS studies of R6G is direct evidence that the chemical binding of R6G to a silver nanoparticle surfaces causes frequency shifts and/or intensity changes in the Raman scattering intensities of specific modes, especially those involving vibrations of the ethylamine moiety. The theoretical work described in this chapter directly addresses this issue by calculating Raman spectra for R6G interacting with a 20-atom silver cluster, and with a flat Ag(111) surface. Tetrahedral Ag_{20} is chosen for part of these studies as it provides a model nanoparticle structure that has a well-defined fragment of a (111) surface, as well as having edges and vertices that can be used to model coordinately unsaturated sites on a particle. In addition, Ag_{20} has been found to provide a reasonable reference structure for determining the chemical contribution to SERS enhancements.[1] Two different geometries of the Ag_{20}/R6G system are considered in the present study, corresponding to two different binding configurations of R6G to a pristine Ag(111) surface. In addition, we study adsorption of R6G on a flat Ag(111) surface of using plane wave DFT calculations to determine optimized geometries and normal mode properties.

1.2 Methods and Computational Approaches

For R6G bound to a Ag_{20} cluster, simple molecular mechanics calculations using the Universal Force field [7] implemented in the software Avogadro[8] were performed to roughly optimize the binding geometry in two configurations: a configuration with the xanthene plane perpendicular to the (111) face of the Ag_{20} cluster, and geometry with the xanthene plane parallel to the face of the Ag_{20} cluster. These two configurations are represented in figure 1.A and 1.B. Subsequently, a Hessian calculation was performed using DFT, a triple ζ with polarization (TZP) basis set, and the Becke-Perdew (BP86)[9,10] exchange-correlation functional. The BP86 exchange-correlation functional was chosen because it has been shown to result in harmonic vibrational frequencies that more closely match experimental results without incorporating a scaling factor.[11] Given the very simplistic model of geometry optimization, some

imaginary frequencies were found in the system, indicating that the structure is not at a local minimum. Since the imaginary frequencies refer to intermolecular modes and modes of the silver cluster that have not been studied in the TERS measurements, we have ignored this problem in the present work. To determine Raman spectra, normal Raman spectroscopy (NRS) calculations were performed using the Amsterdam Density Functional (ADF) 2013.01 program and the AOResponse module implemented in ADF, [12-14] following the method described by Jensen et al.[15] The wavelength of the perturbation used was the standard excitation wavelength used in the measurements, 785 nm. This wavelength is such that the R6G cannot be resonantly excited, which means that the Raman spectrum is in the low frequency limit where intensities are primarily a measure of the static chemical contribution to the SERS enhancement.[1] A damping parameter γ=0.004 au (approximately 0.1 eV) was used, consistent

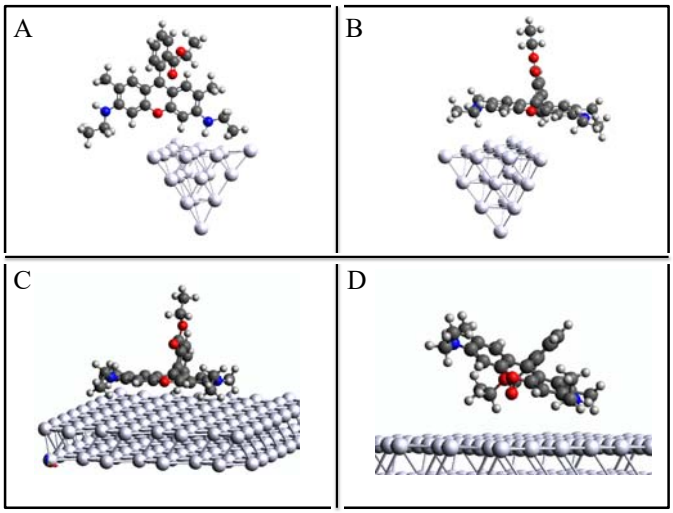

Figure 1: The four different configuration of R6G bound to a silver cluster or silver surface. A: The xanthene plane is oriented perpendicular to the Ag_{20} cluster (configuration $C_{\perp}$), B: The xanthene plane is oriented parallel to the Ag_{20} cluster ($C_{\parallel}$), C: The xanthene plane is oriented parallel to a Ag(111) surface (D1), D: The normal vector from the xanthene plane is oriented 28° from the normal of the Ag(111) surface (D2).

with previous work. [15-18] The zero order regular approximation (ZORA)[19,20] was applied to the calculation of the polarizability tensors and energy convergence values for the AOResponse module were set to 10^{-8} hartree.

In addition to using ADF with a finite cluster model for the silver surfaces, geometry optimization calculations of R6G binding to a flat silver surface using a periodic DFT approach have been performed [21] and are depicted in figures 1.C and 1.D. In these calculations a two-layer deep (111) silver surface slab was used. The Vienna Ab initio Simulation Package (VASP)[22] and DFT with the PBE exchange-correlation functional[23] and a triple zeta basis set was used to determine likely binding geometries of R6G to the silver surface and to calculate the vibrational Hessian matrix. These vibrational modes were then used to calculate the Raman response from the polarizability derivatives using the AOResponse module in ADF. The level of theory was the same as was used for calculating the Raman response for the system consisting of R6G and a Ag_{20} cluster, with the BP86 exchange correlation functional and a TZP basis set. This alternative approach of calculating the vibrational Hessian with the plane-wave VASP software and using the normal modes as input to the polarizability tensor calculations accomplished with ADF will be referred to as `Hessian: VASP/ Polarizability: ADF' approach and thus distinguished from the traditional methodology of computing both the Hessian and the polarizability tensors with ADF, referred to as `Hessian: ADF/ Polarizability: ADF'.

Also investigated was the approximation that the chemical effect on the Raman scattering due to binding to the silver surface predominantly affects the frequencies of the normal modes and minimally effects in the polarizability. This approximation is accomplished by calculating the vibrational modes with the silver present and eliminating the silver atoms, leaving only the R6G molecule for the polarizability calculation. This second method for evaluating polarizability derivatives will be referred to as the ‘polarizability sans-metal’ technique. This technique was applied with both ADF and VASP.

1.3 Results and Discussion

To establish that the VASP/ADF approach compares well to the ADF/ADF approach for computing Raman scattering spectra, the normal Raman scattering of gas phase R6G was computed and is compared in figure 2. The two spectra are in excellent agreement with a small exception in two regions. There is evidence of peak splitting at 1250 cm^{-1} and a slight red shift at 1480 cm^{-1} from the VASP calculations. These slight changes are very minor and overall, the two spectra compare favorably enough to proceed with this methodology for the R6G-Ag systems. The gas phase calculations also compare favorably with previous resonance Raman modeling of R6G performed by Jensen and experimental spectra collected by Klingsporn.[3,5]

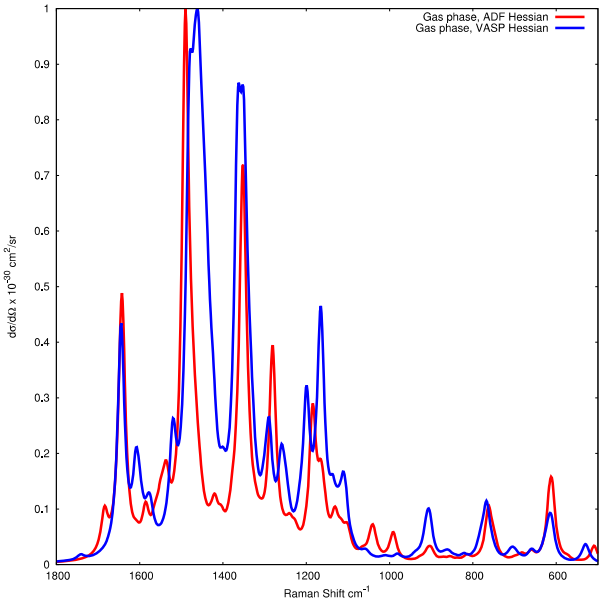

Figure 2: The normalized Resonance Raman scattering spectra of gas phase R6G with a 785 nm excitation with the vibrational frequencies calculated by ADF (blue) and VASP (red).

Geometry optimization studies (with VASP) of R6G binding to a pristine Ag (111) surface resulted in numerous optimized structures.. Two representative geometries were used to perform normal Raman scattering calculations for the normal modes of R6G. For points of comparison, the Raman scattering from R6G in two different binding geometries to a Ag_{20} cluster were also considered (with ADF), one with the xanthene plane in a parallel configuration to the cluster's face, and another geometry with the xanthene plane perpendicular to the face.

Figure 3 summarizes the resonance Raman calculations of the systems referenced in table 1. The first two panels show the ADF versus VASP comparison for gas phase spectra described above in Fig. 2. The 3rd and 4th panels show spectra for the two $C_{\parallel}$ calculations in table 1, while the 5th and 6th panels refer to the $C_{\perp}$ calculations. The 7th and 8th panels refer to the two VASP conformations D1 and D2 in Table 1. The binding configuration that shows the greatest Raman sensitivity is the R6G bound in a parallel configuration to the Ag_{20} face ($C_{\parallel}$). These spectra are very different from the predicted spectra for the perpendicular binding configuration ($C_{\perp}$). Spectral features that change the most are associated with the in-plane and out-of-plane xanthene ring distortions. This may indicate that the resonance Raman scattering signal will be sensitive to small clusters or defect sites on the silver surface and not as sensitive to changes in the binding geometry on pristine silver surfaces. However we note that the experimental spectra are most like the $C_{\perp}$ results, so the $C_{\parallel}$ structures must not be present in significant amounts when R6G adsorbs onto silver particles.

The ‘polarizability sans-metal' approximation simplifies the calculation of the Raman scattering by incorporating the silver cluster in only the vibrational frequency calculations and eliminating the cluster in the polarizability calculations. By making this approximation, we assume that the chemical effect of an organic molecule binding to a silver cluster predominantly affects the frequency of the vibrational modes but has minimal effect on the derivative of the polarizability with respect to the displacement of the normal modes. The

third and fourth, and fifth and sixth panels of figure 3 compare these two methods. The results are qualitatively very similar regardless of whether the silver is present during the polarizability calculations or not. Only the intensity of a few select modes seems to be sensitive to the presence of the silver cluster, notably the vibrations at 1650, 1120, and 810 cm^{-1} which all have some ethyl amine vibrational character. The consistency of the spectra after the `sans-metal' approximation indicates that the majority of the chemical effect in the normal Raman response is due to structural changes in the molecule that lead to shifts in the frequencies of the vibrational modes.

The seventh and eighth panels of figure 3 have been calculated using VASP to identify local energy minimum for R6G binding to a pristine silver surface as well as the Hessian of that system. The Raman response was subsequently calculated at the same level of theory as the previous six panels with ADF, but using the 'sans metal' technique. Both the D1 and D2 configurations yield similar Raman response spectra with the most marked difference being a small peak at 1450 cm^{-1} for configuration D1. There are subtle differences between the Raman response spectra of the D1 and D2 configurations on the silver surface when compared to the Raman response of gas phase R6G, most notably the region between 1300 and 1350 cm^{-1} which corresponds to xanthene ring stretching coupled to hydrogen bending modes on the ethylamine. We also note that panels 7 and 8 show roughly similar spectra to panels 5 and 6, so these VASP-based structures are consistent with the perpendicular conformation

.

Table 2 summarizes the peak assignments for the vibrational modes, here comparing the gas phase results, the $C_{\parallel}$ and $C_{\perp}$ results from panels 3 and 5, and the experimental results (mostly RT TERS, but LT TERS included for two modes with significant ethylamine character) from Klingsporn.[3] The comparison of gas phase results with RT experiment is similar to that presented previously,[3] so the important new results in the work are the frequency shifts in going from gas phase to Ag_{20} results. Also, we have already argued that the $C_{\parallel}$ results are not representative of what is found in the experiment, so this column can be ignored. Looking at the $C_{\perp}$ results, we see that there are generally small frequency shifts in going from the gas phase to Ag_{20} frequencies, however the mode at 1352 cm^{-1} (gas phase) shifts blue by 16 cm^{-1} upon adsorption on Ag_{20}, which is a similar shift but in the opposite direction to

what is seen in the experiment for that mode. Another comparison is with the mode at 1578 cm^{-1} (gas phase). This shifts blue by 10 cm^{-1} in the calculations, which is similar to a 9 cm^{-1} blue shift seen in the experiment. While these comparisons at least show shifts that are similar in magnitude, a more general comparison between theory and experiment is at best qualitative, and not particularly better for the Ag_{20} results than for the gas phase comparison.

Table 1. Rhodamine 6G and Ag systems of varying binding geometries evaluated with indicated software packages and the sans-metal approximation.

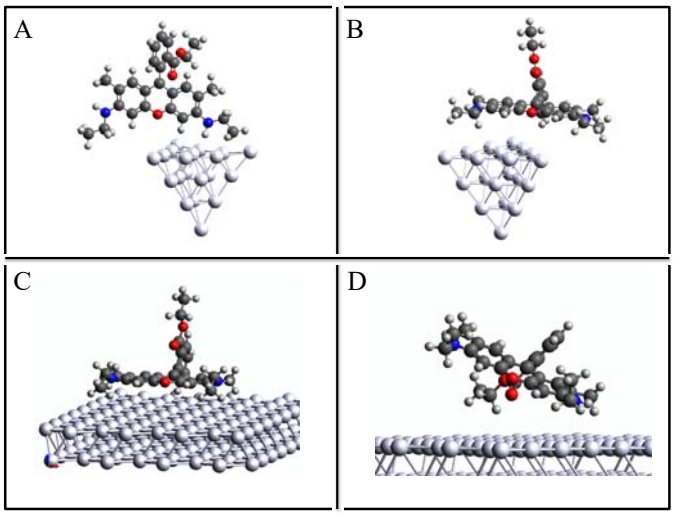

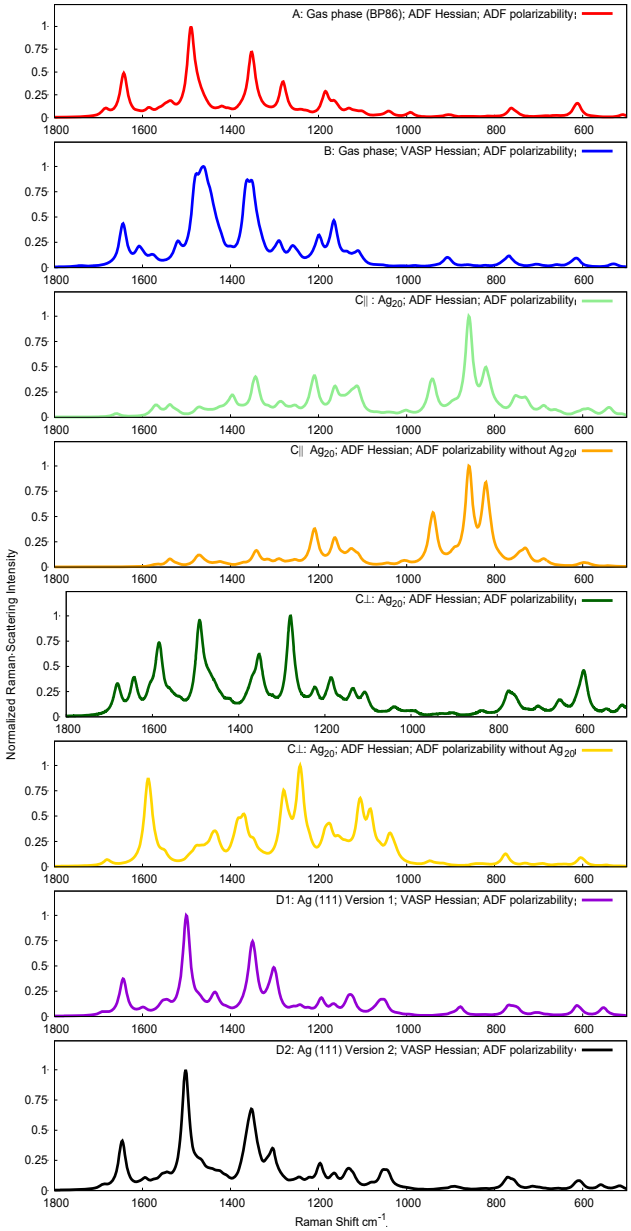

Figure 3: The normal Raman scattering spectra of R6G species listed in table 1. Note that the panels are ordered differently than in Table 1 as indicated in the legends.

Table 2: NRS Calculations of the Raman response of R6G (gas phase) and R6G-Ag_{20} and Experiment.[3] Key: ip=in plane motion, op=out of plane, st=stretch, b=bend, w=wag (symmetric bending), XR=xanthene ring; XRD=xanthene ring distortions, XRS=xanthene ring stretching; EA= ethyl amine; BRS=benzoate ring stretch. All numbers are in cm^{-1} units.

Stretch	R6G	R6G-Ag_{20} Parallel	R6G-Ag_{20} Perpendicular	Experiment[3]
ip XRD		600	605	625
op XRD	616	538		625
ip XRD	762		775	775
w H-XR	1184	1112-1163	1106-1184	1175-1200
XRD, w H-XR	1280	1283	1279	1310-1325
XRS, w H-ethane	1352		1368	1350-1375 (LT shifts red by 14)
w H-N, b CH on EA	1490	1395	1493-1441	
XRD	1508	1522		
XRD ip, b. HN, BRS	1578 (v.w.)	1538-1569	1588	1538 (LT-TERS shifts blue by 9)
XRS	1643	1569		1640-1660
CO st.	1648	1659	1680	1660

1.4 Conclusions

The chemical effect of binding R6G to a silver surface and a silver nanoparticle model have been investigated. Since most of the bright modes in the gas phase R6G spectrum involve vibrations in the xanthene ring, and it is predicted through simple geometry optimizations that R6G binds to a silver surface through that ring, it is not surprising that there are noticeable spectral changes upon binding to the metal surface. Indeed, the most significant changes are for a structure where the xanthene ring is parallel to the surface, however the spectra we obtain for this structure are quite different from the experiment so we assume this is not significantly populated in the expeirment. Qualitative comparisons with experiment are found when the xanthene is perpendicular to a Ag_{20} cluster. In this case we found shifts in vibrational frequencies due to adsorption that are similar in magnitude to those seen experimentally. However the overall appearance of the spectrum is not in better agreement with experiment than the gas phase calculated spectrum.

Another result of this paper is that we have explored two new methodologies for calculating spectra for adsorbed molecules that provide useful simplifications for what is generally a very complicated calculation. In the first, we considered an approach that couples a vibrational frequency calculation performed with the plane-wave DFT based software package, VASP, to polarizability calculations performed with the AOResponse module implemented in ADF. The second methodology was the `sans-metal' approach and it was confirmed that the spectral changes upon elimination of the metal during the polarizability calculations usually have a minimal effect on the off resonant Raman spectra. From this study, it seems that the majority of the effect of binding R6G to a silver substrate can be captured by optimizing the R6G geometry and performing the Hessian calculation in the presence of a silver cluster or surface. However the lack of agreement between details of the calculated spectrum and experiment indicates the structural models we have used are still inadequate.

Acknowledgment

This research was supported by the NSF GRFP under Grant DGE-1324585, Department of Energy grant DE-FG02-10ER16153 (for methods development), and by AFOSR MURI grant FA9550-14-1-0003 (applications).

1. Valley, N., Greeneltch, N., Van Duyne, R. P., Schatz, G. C. (2013) A look at the origin and magnitude of the chemical contribution to the enhancement mechanism of surface-enhanced Raman spectroscopy (SERS): theory and experiment, J. Phys. Chem. Lett. 4, pp. 2599-2604.

2. Aikens, C. M.; Schatz, G. C. (2006) TDDFT studies of absorption and SERS spectra of pyridine interacting with Au_{20},J. Phys. Chem. A 110, pp.13317-13324.

3. Klingsporn, J. M., Jiang, N., Pozzi, E. A., Sonntag, M. D., Chulhai, D., Seideman,T., Jensen, L., Hersam, M. C., Van Duyne, R. P. (2014) Intramolecular insight into adsorbate-substrate interactions via low-temperature, ultrahigh-vacuum tip-enhanced Raman spectroscopy, J. Am. Chem. Soc. 136, pp. 3881-3887.

4. Camden, J. P., Dieringer, J. A., Wang, Y., Masiello, D. J., Marks, L. D., Schatz, G. C., Van Duyne, R. P. (2008) Probing the structure of single molecule surface-enhanced Raman scattering hot spots, J. Am. Chem. Soc. 130, pp. 12616-12617.

5. Jensen, L., Schatz, G. C. (2006) Resonance Raman scattering of Rhodamine 6G as calculated using time-dependent density functional theory, J. Phys. Chem. A, 110, pp. 5973-77.

6. Liu, S., Wan, S., Chen, M., and Sun, M. (2008). Theoretical study on SERRS of rhodamine 6G adsorbed on Ag_2 cluster: chemical mechanism via intermolecular or intramolecular charge transfer, J. Raman Spectrosc 39, pp. 1170–1177.

7. Rappe, A. K.,Casewit, C. J.,Coldwell, W. A., and Skiff, W. M. (1992). UFF, a full periodic table force field for molecular mechanics and molecular dynamics simulations, J. Am. Chem. Soc., 114, pp. 10024–10035.

8. Hanwell, M. D., Curtis, D. E., Lonie, D. C., Vandermeersch, T., Zurek, E., and Hutchison, G. R. (2012). Avogadro: an advanced semantic chemical editor, visualization, and analysis platform, J. Chem. Inf. 4, pp. 17.

9. Becke, A. D. (1988). Density-functional exchange-energy approximation with correct asymptotic behavior, Phys. Rev A, 38, pp. 3098–3100.

10. Perdew, J. (1986). Density-functional approximation for the correlation energy of the inhomogeneous electron gas, Phys. Rev. B 33, pp. 8822–8824.

11. Neugebauer, J. and Hess, B. A. (2003). Fundamental vibrational frequencies of small polyatomic molecules from density-functional calculations and vibrational perturbation theory, J. Chem. Phys. 118, pp. 7215.

12. ADF2013, SCM, Theoretical Chemistry, Vrije Universiteit, Amsterdam, The Netherlands, http://www.scm.com/.

13. Guerra, C. F., Snijders, J. G., Te Velde, G., and Baerends, E. J. (1998). Towards an order-N DFT method. Theor. Chem. Acc. 99, pp. 391–403.
14. Te Velde, G., Bickelhaupt, F. M., Baerends, E. J., Fonseca Guerra, C., van Gisbergen, S. J., Snijders, J. G., and Ziegler, T. (2001). Chemistry with ADF, J. Comput. Chem., 22, pp.931–967.
15. Jensen, L., Autschbach, J., and Schatz, G. C. (2005). Finite lifetime effects on the polarizability within time-dependent density-functional theory, J. Chem. Phys.122, pp. 224115–224115.
16. Jensen, L., Zhao, L. L., Autschbach, J., and Schatz, G. C. (2005). Theory and method for calculating resonance Raman scattering from resonance polarizability derivatives, J. Chem. Phys.123, pp. 174110–174110.
17. Greeneltch, N. G., Davis, A. S., Valley, N. A., Casadio, F., Schatz, G. C., Van Duyne, R. P., and Shah, N. C. (2012). Near-Infrared Surface-Enhanced Raman Spectroscopy (NIR-SERS) for the Identification of Eosin Y: Theoretical Calculations and Evaluation of Two Different Nanoplasmonic Substrates, J. Phys. Chem. C, 116, pp. 11863–11869.
18. Aquino, F. W. and Schatz, G. C. (2014). Time-dependent density functional methods for Raman spectra in open-shell systems, J. Phys. Chem. A, 118, 2, pp. 517-525.
19. van Lenthe, E., Baerends, E. J., and Snijders, J. G. (1993). Relativistic regular two-component Hamiltonians, J. Chem. Phys, 99, pp. 4597.
20. van Lenthe, E., Aikens, C. M., Baerends, E. J., Li, S., Snijders, J. G., and Schatz, G. C. (1994). Relativistic total energy using regular approximations, J. Chem. Phys., 101, pp. 9783–9792.
21. Fu, B., Van Dyck, C., Zaleski, S. Van Duyne, R.P., and Ratner, M.A. (Submitted). Single Molecule Electrochemistry: Impact of Surface Site Heterogeneity.
22. Kresse, G. and Furthmüller, (1996). Efficiency of ab-initio total energy calculations for metals and semiconductors using a plane-wave basis set, Comput. Mater. Sci., 6, pp. 15–50.
23. Perdew, J. P. and Burke, K., Ernzerhof, M. (1996). Generalized Gradient Approximation Made Simple, Phys. Rev. Lett., 77, pp. 3865– 3868.